Hematopoietic Progenitor Cell Rolling in Bone Marrow Microvessels: Parallel Contributions by Endothelial Selectins and Vascular Cell Adhesion Molecule 1

By Irina B. Mazo,* Jose-Carlos Gutierrez-Ramos,‖ Paul S. Frenette,*§ Richard O. Hynes,¶ Denisa D. Wagner,*‡ and Ulrich H. von Andrian*‡

*From *The Center for Blood Research, the ‡Department of Pathology, and the §Department of Medicine, Harvard Medical School, Boston, Massachusetts 02115; ‖Millenium Pharmaceuticals, Inc., Cambridge, Massachusetts 02139; and the ¶Howard Hughes Medical Institute, Massachusetts Institute of Technology, Cambridge, Massachusetts 02139*

Summary

We have used intravital microscopy to study physiologically perfused microvessels in murine bone marrow (BM). BM sinusoids and venules, but not adjacent bone vessels, supported rolling interactions of hematopoietic progenitor cells. Rolling did not involve L-selectin, but was partially reduced in wild-type mice treated with antibodies to P- or E-selectin and in mice that were deficient in these two selectins. Selectin-independent rolling was mediated by α4 integrins, which interacted with endothelial vascular cell adhesion molecule (VCAM)-1. Parallel contribution of the endothelial selectins and VCAM-1 is not known to direct blood cell trafficking to other noninflamed tissues. This combination of constitutively expressed adhesion molecules may thus constitute a BM-specific recruitment pathway for progenitor cells analogous to the vascular addressins that direct selective lymphocyte homing to lymphoid organs.

Key words: bone marrow • selectins • α4 integrin • intravital microscopy • homing

The bone marrow (BM)[1] is a site of intense cellular traffic from the hematopoietic compartment to the peripheral blood and vice versa. This vital process requires the formation and release of adhesive bonds between blood cells and BM stroma cells in both the extra- and intravascular space. Some adhesion molecules recently have been implicated in the release of hematopoietic stem cells into the systemic circulation (1, 2). However, little is known about the adhesion pathways that are involved in the homing of hematopoietic stem cells and hematopoietic progenitor cells (HPCs) from the blood to the BM. It is likely that a critical step in this process is the adhesion of blood-borne cells to the lining of BM microvessels in the presence of physiologic fluid shear that is exerted by the blood stream. Extensive studies on mature leukocytes in the microcirculation of a number of other organs have demonstrated that cells must undergo a sequence of distinct adhesion steps to accumulate in a tissue (3, 4). Most adhesion cascades are initiated by a primary tethering event mediated by selectins and their carbohydrate ligands that allows cells to roll slowly along the wall of postcapillary venules. Subsequently, when a rolling cell encounters a chemoattractant that binds to surface receptors, an intracellular signaling cascade is triggered that induces the functional upregulation of integrins. Integrins then bind to endothelial counterreceptors, mediating firm arrest of the rolling leukocyte. Subsequently, leukocytes migrate through the blood vessel wall and enter the extravascular tissue.

Due to the anatomic inaccessibility of most BM microvessels, it is not known whether a similar multistep process can also occur in BM microvessels. A detailed knowledge of these events is important since the success of BM and stem cell transplantations depends on the efficient seeding of grafted cells in the recipient's BM. BM transplantation studies have shown that the α4 integrin/vascular cell adhesion molecule (VCAM)-1 (CD49d/CD106) pathway and one or more unidentified lectins determine in part the recovery of colony-forming units from the BM of irradiated mice (5, 6). However, little is known about the site of action and the mechanisms through which these and perhaps other molecules contribute to HPC homing. Recent data indicate that murine and human BM endothelium

[1]*Abbreviations used in this paper:* BM, bone marrow; BV, bone venule; CN, capillary network; CV, collecting venule; FDCP-mix, factor-dependent cells Paterson-mix; FL, fetal liver; F/P, fluorescein/protein; HPC, hematopoietic progenitor cells; IV, intermediate venule; PSV, postsinusoidal venule; VCAM, vascular cell adhesion molecule.

J. Exp. Med. © The Rockefeller University Press • 0022-1007/98/08/465/10 $2.00
Volume 188, Number 3, August 3, 1998 465–474
http://www.jem.org

constitutively expresses VCAM-1 (7, 8), suggesting that VCAM-1 may be involved in the trafficking of cells between blood and BM.

The role of selectins in HPC trafficking is also unclear. Evidence that carbohydrate–protein interactions may be involved in homing of HPCs to BM was acquired some time ago (6). It is known that L-selectin is expressed on the majority of HPCs (9-11), but its function on these cells is unclear. No hematopoietic defects have been described in L-selectin knockout mice (12). HPCs were also shown to bind to P-selectin (13), although the expression of P-selectin on BM endothelial cells has not been described. Recent data suggest that E-selectin is constitutively expressed on endothelial cells of human and murine hematopoietic tissues (8, 14), but the role of E-selectin in HPC homing has not been addressed.

We describe a novel technique to visualize and dissect interactions of HPCs with BM microvessels in the skulls of anesthetized mice. This model allows the direct microscopic observation and quantitative analysis of adhesion events in physiologically perfused BM microvessels. Using this approach, we have characterized the anatomy and hemodynamics of the skull BM microvasculature, and we demonstrate that HPCs roll in BM venules and sinusoids in the absence of inflammation. Using neutralizing antibodies and genetically deficient mice, we show that HPC rolling is mediated by parallel contributions of constitutively expressed P- and E-selectin and VCAM-1.

Materials and Methods

Antibodies. Anti-α4 mAb PS/2, anti-LFA-1 mAb Tib 213, anti–L-selectin mAb Mel-14, and anti–MAdCAM-1 mAb Meca-367 were provided by Dr. E.C. Butcher (Stanford University, Stanford, CA). Anti–VCAM-1 mAb MK 2.7, anti–P-selectin mAb 5H1, and anti–E-selectin mAb 10E6 were a gift from Dr. B. Wolitzky (Hoffmann-La Roche Inc., Nutley, NJ). All mAbs were purified from hybridoma supernatants and stored at −70°C in LPS-free saline. Aliquots of mAbs Meca-367 and MK 2.7 were fluoresceinated with carboxyfluorescein succinimidyl ester (Molecular Probes, Eugene, OR). Fluorescein/protein (F/P) ratios were 6.94 and 2.85, respectively. FITC- and PE-conjugated mAbs to murine c-kit, Ter-119, Mac-1, and CD34 were purchased from PharMingen (San Diego, CA). FITC- and PE-labeled goat anti–rat IgG was from Caltag Labs. (South San Francisco, CA).

Cells. The murine progenitor cell lines factor-dependent cells Paterson-mix (FDCP-mix) and M1 were grown as previously described (15, 16). For in vivo experiments, cells were fluorescently labeled with 2′,7′-bis-(carboxyethyl)-5(and-6) carboxyfluorescein (BCECF; Molecular Probes). After staining for 30 min at 37°C (2 μg BCECF/10^7 cells), cells were washed and resuspended to 10^7 cells/ml in RPMI 1640 (BioWhittaker, Walkersville, MD) containing 10% fetal bovine serum.

To generate fetal liver (FL) HPCs, female and male C57BL/6J mice were mated following standard procedures. Pregnant females were killed 11 d after first observation of a vaginal plug. FLs were dissected from embryos and sieved through a nylon mesh (Becton Dickinson, San Jose, CA). Cells were washed and resuspended in IMDM (BioWhittaker), and viability was determined by trypan blue exclusion. Fluorescent labeling with BCECF was as described for FDCP-mix cells.

Unlabeled aliquots of cell lines and FL cells were transferred to ice for mAb staining and flow cytometric analysis of surface molecules; all other cells were kept at 37°C throughout the experiment.

Fluorescently labeled red blood cells from C57/Bl6J donor mice were used to assess BM microhemodynamics. 0.5 ml of anticoagulated blood was washed in 1.0 ml PBS, resuspended in PBS to a 10% hematocrit (based on pellet size), layered on Histopaque-1077 (Sigma Chemical Co., St. Louis, MO), and centrifuged for 8 min at 900 rpm to remove leukocytes. The pellet was resuspended to a 5% hematocrit in DMEM (BioWhittaker) with glucose, and 0.5 mg/ml BCECF was added. The cells were incubated at 37°C for 40 min, washed, and resuspended to 5% hematocrit in PBS for injection.

Animals. Adult C57/Bl6J×129S mice of both sexes were used in these studies. P/E-selectin double knockout mice on the same genetic background have been described previously (14). Animals were kept in a viral antigen–free barrier facility on standard lab chow and sterile water supply ad libidum. This study complies with National Institutes of Health guidelines for the care and use of laboratory animals.

Animal Preparation. Mice were anesthetized by intraperitoneal injection (10 ml/kg) of physiologic saline containing ketamine (5 mg/ml) and xylazine (1 mg/ml). The hair in the submandibular area of the neck and on the skullcap was removed using hair removal lotion (Nair, Carter Products, NY). PE-10 polyethylene catheters (Becton Dickinson) were inserted into the left jugular vein for administration of fluids and into the right common carotid artery for injection of fluorescent cells into the aortic arch. The scalp was incised in the midline and the frontoparietal skull was exposed while carefully avoiding damage to the bone tissue. A plastic ring was inserted in the incision to spread the skin and to allow application of sterile physiologic saline solution to prevent drying of the tissue. To immobilize the animal's head, the mouse was placed on a customized plexiglas stage equipped with a stereotactic holder (David Kopf Instruments, Tujunda, CA).

Intravital Microscopy. An intravital microscope (IV 500; Mikron Instruments, San Diego, CA) equipped with water immersion objectives (Carl Zeiss, Inc., Thornwood, NY) was used in experiments. Small boluses (~50 μl) of BCECF-labeled cells were injected through the right carotid artery catheter. Fluorescent cells were visualized in the left frontoparietal skull by video-triggered stroboscopic epi-illumination (Chadwick Helmuth, El Monte, CA) through an FITC filter set and an ×10 objective (Zeiss Achroplan, numerical aperture [NA] 0.3 ∞, Water). 150 kD of FITC dextran (Sigma Chemical Co.) was injected in some experiments for measurements of microvascular dimensions using an ×40 objective (Zeiss Achroplan, NA 0.75 ∞, Water) as previously described (17). At the end of some experiments, saline containing 1 mg/ml rhodamine 6G or 4 mg/ml rhodamine 123 (Molecular Probes) was injected intravenously at a dose of 1.5 ml/kg body weight. The distribution of FITC-dextran (Sigma Chemical Co.) and rhodamine compounds in the skull was recorded through an ×4 objective (Achroplan, NA 0.16). All scenes were recorded on video tape using a SIT camera (VE 1000-SIT; Dage MTI, Michigan City, IN), a time base generator (For - A, Montvale, NJ), and a Hi-8 VCR (Sony, Boston, MA).

Image analysis. 62 representative BM venules and sinusoids were analyzed to measure luminal cross-sectional diameter and velocity of labeled erythrocytes (≥20 cells/vessel) using a PC-based image analysis system (18). The wall shear rate was calculated for each venule as previously described (17, 19). Rolling fractions of progenitor cell lines and FL HPCs were determined by counting the number of interacting cells in each venule or sinusoid per 100 cells that passed through the same vessel during an injection.

Histology. The frontoparietal bones of murine skulls were explanted and fixed for 6 h in PBS containing 4% paraformaldehyde, decalcified (Accumate RDO; Sigma Chemical Co.) and embedded in paraffin in a Tissue-Tec vacuum infiltration processor (Miles Labs., Inc., Somerset, MA). Frontal sections were cut (5-μm thick) with a microtome (Reichert-Jung, Nussloch, Germany) and stained with hematoxylin and eosin following standard procedures.

Culture Colony-Forming Unit Assay. Frontoparietal bones, femora, and brains of five mice were ground using a mortar and pestle. Single cell suspensions were generated and mononuclear cells (MNCs) were isolated by density gradient centrifugation over Ficoll-Hypaque (Sigma Chemical Co.). Colonies were grown in IMDM containing 15% fetal bovine serum (JRH Biosciences, Lenexa, KS), 1% bovine serum albumin (Sigma Chemical Co.), 0.13 mM β-mercaptoethanol (Sigma Chemical Co.), 2.5 U/ml recombinant erythropoietin (Amgen, Inc., Thousand Oaks, CA), 150 ng/ml recombinant mouse stem cell factor (Sigma Chemical Co.), and 10% (vol/vol) ×63 IL-3–conditioned medium. Isolated MNCs, 1 ml/well, were plated in duplicate in 0.9% methylcellulose (Sigma Chemical Co.) at 10^5 and 3×10^5 cells/ml. Cultures were maintained at 37°C in 5% CO_2. Colonies were counted after 8 d.

FACS® Analysis. Surface expression of adhesion molecules by FDCP-mix, M1, or FL HP cells was assessed by flow cytometry: the cells were suspended to 10^7 cells/ml in RPMI 1640 and kept on ice; 20 μg/ml of mAbs to L-selectin, α4, LFA-1, Mac-1, β7, cutaneous lympohocyte antigen (CLA), and P-selectin glycoprotein ligand (PSGL)-1 were added to 100 μl cell suspension. Cells were washed twice after 30 min of staining, and FITC- or PE-conjugated goat anti–rat IgG was added in a dilution of 1:100 or 1:200, respectively. Subsequently, cells were washed twice after 30 min of staining and analyzed using a FACScan® flow cytometer (Becton Dickinson). For two-color flow cytometry cells were incubated with 1:200 diluted rat sera (Sigma Chemical Co.) for 15 min on ice to decrease nonspecific binding of antibody and washed. Subsequently cells were incubated on ice with PE- and FITC-conjugated mAbs (30 min each incubation) with two washings between each incubation.

Statistical Methods. For statistical comparison of two samples, a two-tailed Student's *t* test was used when applicable. Multiple comparisons were performed using the Kruskal-Wallis test with Bonferoni correction of *P*. Differences were considered statistically significant when $P < 0.05$. Data are presented as mean ± SEM unless indicated otherwise.

Results and Discussion

Anatomy of the Microcirculation in the Murine Frontoparietal Skull. We noticed that the flat bones which form the skull's calvaria contain BM that was macroscopically visible as a red coloration, primarily in the parasagittal region (Fig. 1 *A*, *left*). Visually identified red BM was located often in the interparietal bone parallel to the lambdoidal suture, but the microvascular network in this area was frequently sparse and poorly visible. In contrast, the thin layer of bone that covered the BM cavities in the frontoparietal skull was sufficiently transparent to allow the observation of a multitude of underlying microvessels without the need for surgical manipulation of the bone itself. Thus, the microvascular network in this area of the skull could be studied in the absence of trauma-induced hemorrhage or significant inflammation.

To characterize the microvascular anatomy, we intravenously injected FITC-dextran, an inert plasma marker that facilitates measurements of luminal dimensions (17) (Fig. 1 *A*, *right*). Although there was considerable heterogeneity between animals, several distinguishing features of the frontoparietal skull microcirculation were noted. The most prominent vessel was a large collecting venule (CV) that was often macroscopically detectable. This venule was bilaterally located in the frontal bone in close proximity and parallel to the coronal suture and drained into the superior sagittal sinus. The function of this venule may be analogous to that of the central vein in the BM of long bones. The BMCV received afferent blood from a parietal network of sinusoids that were irregularly shaped, frequently arranged in a honeycomb pattern, and linked by short anastomoses. The direction of blood flow in some of these anastomosing vessels fluctuated unpredictably. Most laterally positioned sinusoids drained directly into the BMCV, whereas blood from medially located sinusoids reached the BMCV via one or more postsinusoidal venules (PSV). BMCV also received blood from laterally located venules in the frontal bone. These vessels included both elongated bone venules (BV) that had few branches and no apparent contact to BM cavities and a number of intermediate venules (IV) with numerous branches that were surrounded by a variably thick layer of BM tissue. Diameters of BMCV, sinusoids, and BMPSV did not differ significantly from each other, whereas BMIV were more narrow (Table 1).

In addition to the vessels described above, we noted parasagittal capillary networks (CNs) in the frontal and interparietal bones. Blood flow in CN vessels (diameter: 10.9 ± 2.2 μm, mean ± SD) was typically low and highly variable and was often partially obscured by extravascular erythroid cells which seemed more concentrated in this area than elsewhere. The adhesive phenomena observed in the frontal CNs were consistent with those from other regions of the skull. However, these data were not included in the results described below because only few cells entered this area and due to poor visibility it was often not possible to distinguish between flow-related slowing and adhesive interactions of cells.

Microvascular Hemodynamics in the Skullcap. To assess BM microhemodynamics, fluorescently labeled murine erythrocytes were injected intraarterially and their velocity in BM venules and sinusoids was determined by off-line video analysis as previously described (17). Mean blood flow velocities and wall shear rates in BM sinusoids, BMPSVs, and BMCVs were similar except in BMIVs, where these parameters were lower (Table 1). These measurements of microvascular hemodynamics and dimensions are in good agreement with earlier studies of blood flow in BM microvessels of the rabbit fibula (20) and with ultrastructural measurements of BM sinusoids in guinea pigs (21).

Intravenously Injected Rhodamine Fluorophores Delineate Hematopoietic Tissue within BM Cavities. Previous studies on the ultrastructure of BM samples have shown that the walls of many microvessels are discontinuous, i.e., they partly lack a basal lamina and adventitial cells (21). However, we did not detect FITC-dextran (150 kD) extravasation from

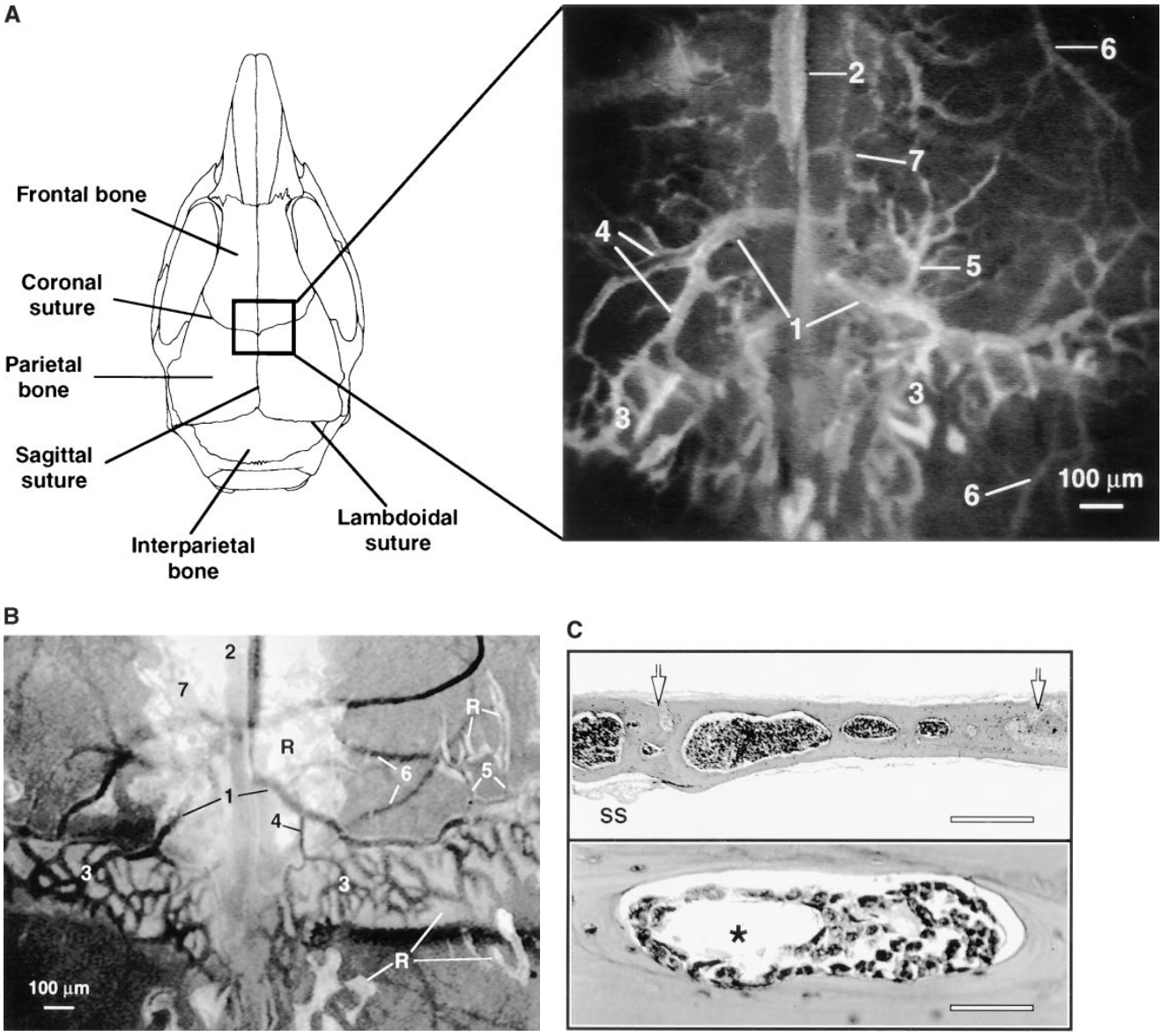

Figure 1. Anatomy and histology of murine skull BM. (*A*) Top view of the dorsal murine skull. Major flat bones and sutures are shown schematically (*left*). The rectangle over the frontoparietal region indicates the area which shows the typical microvascular anatomy after intravenous injection of 150-kD FITC-dextran (*right*). A large BMCV (*1*) in the parietal bone parallel to the coronal suture drains into the sagittal sinus (*2*). A parietal network of sinusoids (*3*) drains into the BMCV, either directly or via one or more BMPSV (*4*). BMCVs also receive blood from laterally located venules in the parietal bone. These vessels include BMIVs (*5*) and some BVs (*6*). A dense parasagittal CN (*7*) is located in the frontal bone. Blood flow in CN capillaries is highly variable and often partially obscured by red marrow, which tends to be more concentrated in this area than elsewhere. (*B*) Rhodamine 6G accumulation. A marked accumulation of the dye (*R*) is observed in the parasagittal regions of frontal and parietal bones and in the perivascular space of sinusoids and some, but not all, venules. Identical staining patterns were seen with rhodamine 123 (data not shown). Number designations are as in *A*. (*C*) Photomicrographs of hematoxylin and eosin–stained frontal sections through the frontal bones of a skull. The sections lie approximately on the long axis of the quadrangle in *A* (*left*). Several intraosseous cavities filled with densely packed hematopoietic cells are shown at low magnification (*top*). Arrows indicate the sagittal (*left*) and coronal (*right*) sutures; *SS*, sagittal sinus. At higher magnification (*bottom*), a microvessel (*) can be detected within a BM cavity. Scale bars in top and lower panels depict 500 and 50 μm, respectively. (*D*) Colony-forming capacity of MNCs from murine brain, skull, and femur. MNCs isolated from brains, skullcaps, and femora of five mice were harvested and plated on methylcellulose. CFU-C assays were performed in duplicate. Data are expressed as mean ± SEM of three independent experiments.

BM vessels, indicating that skull BM endothelium constitutes an efficient barrier to blood-borne macromolecules. In contrast, when the low molecular weight fluorophores rhodamine 6G (479 dalton) or rhodamine 123 (381 dalton) were injected intravenously, intense extravascular labeling was observed in a bizarrely shaped, sharply demarcated, and approximately symmetrical pattern in parasagittal areas of the frontal, parietal, and interparietal bones. Contained within

Table 1. *Dimensions and Hemodynamic Parameters of BM and Bone Microvessels*

Parameters	BMCV	Sinusoids	BMPSV	BMIV	BV
n (venules/animals)	16/5	14/5	5/5	19/5	8/3
Diameter (μm)	98.8 ± 12	41.9 ± 10.8	56.2 ± 11.9	28.8 ± 9.1	21.6 ± 7.9
	(89.3–126.6)	(21.9–60.2)	(47.6–74.8)	(17.0–50.4)	(13.7–36.8)
V_{rbc} (μm/sec)	525.0 ± 293.3	418.0 ± 126.2	508.6 ± 190.9	196.9 ± 153.2	222.7 ± 124.3
	(120.9–1220.1)	(255.1–731.6)	(385.0–842.1)	(88.2–750.2)	(75.3–385.2)
WSR (sec^{-1})	91.7 ± 43.6	91.4 ± 36.9	76.9 ± 19.9	56.9 ± 33.6	98.6 ± 28.5
	(23.7–167.9)	(50.5–164.8)	(54.5–98.1)	(15.2–130.6)	(53.3–144.9)

To assess BM microhemodynamics, fluorescently labeled murine erythrocytes were injected intraarterially and their velocity in venules and sinusoids was determined by off-line video analysis (17). Since rheologic parameters in BMCVs were often different in individual segments of the same venule upstream and downstream of bifurcations, these vascular segments were analyzed separately. V_{RBC}, red blood cell velocity; WSR, wall shear rate. Data are presented as arithmetic mean ± SD, and ranges are given in parentheses.

these regions were the dense CNs, sinusoids, BMPSVs, BMCVs, and BMIVs, but not BVs (Fig. 1 *B*).

The conspicuous staining pattern with rhodamine compounds was unique to the skull calvaria; we did not observe a similar extravascular distribution of rhodamine 6G in other murine tissues including skin, cremaster muscle, lymph node, small intestine, and Peyer's patches, although microvessels in some organs (especially the gut) appear to be similarly permeable to rhodamine 6G (von Andrian, U.H., unpublished data). Therefore, the restricted distribution of rhodamine suggested the presence of anatomically confined compartments. To test this, we performed a histologic examination of coronal sections of paraffin-embedded skull caps (Fig. 1 *C*). The frontoparietal skull contained intraosseous BM cavities that were filled with densely packed hematopoietic cells of various lineages and permeated by numerous microvessels. The intense intravital staining of these areas implies that many cells were metabolically active because both rhodamine compounds preferentially stain mitochondria (22). Indeed, this property of rhodamine 123 has been exploited to assess the degree of HPC differentiation (23).

Murine Skullcap BM Contains Hematopoietic Progenitor Cells. To confirm that skull BM cavities contained HPCs, we performed CFU-C assays in methylcellulose with MNCs isolated from skull caps, femora, and brains of adult mice. In three independent experiments, plated cells from skulls and femora, but not from brains, gave rise to granulocyte/macrophage and erythroid colonies (3,908 ± 238 and 5,331 ± 841 colonies per 10^6 MNCs, respectively, mean ± SEM; Fig. 1 *D*). The commitment of HPCs to these two lineages reflects the composition of growth factors in our assay and does not exclude the presence of lymphoid progenitors and megacaryocytes in the skull. The difference in the frequency of colonies in CFU-C assays using MNCs from skulls and femora was not statistically significant. We conclude that the hematopoietic tissue within the cavities of adult murine calvaria contains HPCs at a similar frequency as the marrow of the long bones.

BM Venules and Sinusoids Support Constitutive Rolling Interactions of FDCP-mix Cells. Having established that we can identify and analyze BM microvessels, we tested the adhesive behavior of FDCP-mix cells, a murine cell line with HPC-like properties. This is a growth factor (IL-3)–dependent multipotential cell line that can proliferate in the presence of horse sera without differentiating (15). Fluorescently labeled cells were injected through a carotid artery catheter and their passage through the BM was recorded (Fig. 2 *A*). FDCP-mix cells rolled in most BM venules and sinusoids, but rarely interacted with BV (Fig. 2 *B*). Within different types of BM microvessels rolling fractions were variable, but they were always significantly higher than in adjacent BVs. We conclude that BM microvessels are distinguishable from BV not only by their shape, localization, and perivascular accumulation of rhodamine compounds, but also by their distinct adhesive properties.

Constitutively Expressed E- and P-selectin, but not L-selectin, Participate in FDCP-mix Cell Rolling in BM Microvessels. Next, we set out to identify the molecular mechanisms of progenitor cell rolling. The three selectins have been shown to mediate rolling of mature leukocytes in many other organs (24). Flow cytometric analysis indicated that FDCP-mix cells express L-selectin, P-selectin glycoprotein ligand (PSGL)-1, and low levels of the cutaneous lymphocyte antigen (CLA; data not shown). The latter two are ligands for endothelial P- and E-selectin, respectively (25, 26). A similar pattern of selectins and their ligands was found on human $CD34^+$ HPCs (13), which supports the validity of using FDCP-mix cells as a model for stem cell trafficking. Treatment of animals and cells with a mAb to L-selectin had no effect (Fig. 2 *C*), whereas mAbs to P- and E-selectin reduced rolling by 58 and 32%, respectively. Importantly, although endothelial cells in other organs such as the mesentery or cremaster muscle may require prior cytokine activation or other inflammatory stimuli to support rolling interactions via endothelial selectins (27–29), BM venules and sinusoids supported FDCP-mix cell rolling constitutively. Although it can not be excluded that the surgical ex-

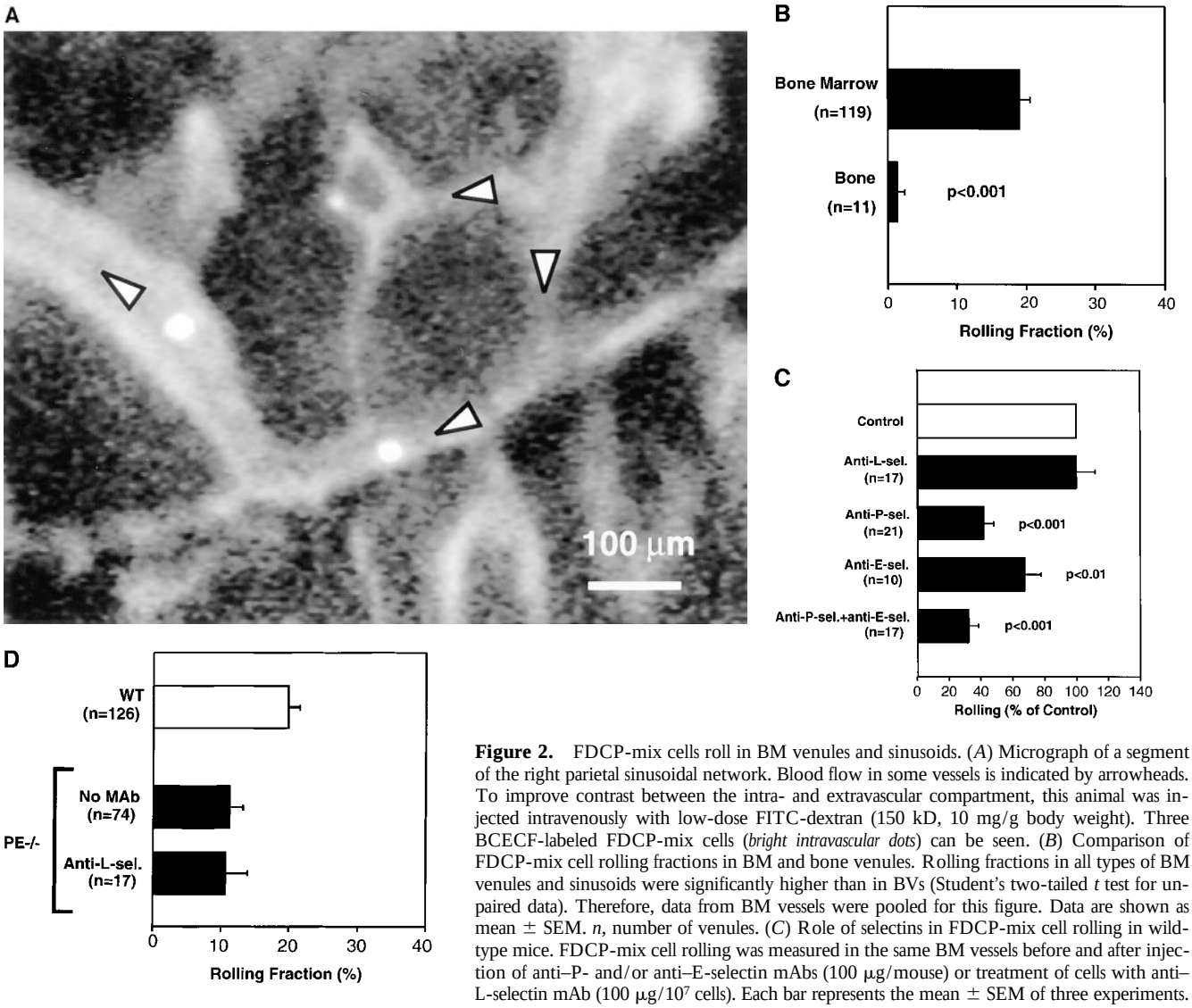

Figure 2. FDCP-mix cells roll in BM venules and sinusoids. (*A*) Micrograph of a segment of the right parietal sinusoidal network. Blood flow in some vessels is indicated by arrowheads. To improve contrast between the intra- and extravascular compartment, this animal was injected intravenously with low-dose FITC-dextran (150 kD, 10 mg/g body weight). Three BCECF-labeled FDCP-mix cells (*bright intravascular dots*) can be seen. (*B*) Comparison of FDCP-mix cell rolling fractions in BM and bone venules. Rolling fractions in all types of BM venules and sinusoids were significantly higher than in BVs (Student's two-tailed *t* test for unpaired data). Therefore, data from BM vessels were pooled for this figure. Data are shown as mean ± SEM. *n*, number of venules. (*C*) Role of selectins in FDCP-mix cell rolling in wild-type mice. FDCP-mix cell rolling was measured in the same BM vessels before and after injection of anti–P- and/or anti–E-selectin mAbs (100 μg/mouse) or treatment of cells with anti–L-selectin mAb (100 μg/10^7 cells). Each bar represents the mean ± SEM of three experiments. *n* corresponds to the number of venules. Groups were compared with control using the Kruskal-Wallis test followed by Bonferoni correction of *P*. (*D*) Comparison of FDCP-mix cell rolling in wild-type and P/E-selectin double knockout mice. Data are expressed as mean ± SEM of three experiments. Rolling fractions in P/E-deficient mice were significantly lower than in wild-type littermates ($P < 0.001$; Student's *t* test), but were not affected by anti–L-selectin mAb (100 μg/10^7 cells). *n*, number of venules.

posure of the skull may have induced some tissue irritation, the time course of these experiments (typically <1 h) was too short for significant transcriptional induction of E-selectin (30). Moreover, inflammation-induced rapid upregulation of P-selectin from Weibel-Palade bodies would likely affect all exposed venules. BVs in immediate vicinity to BM venules and sinusoids did not support rolling, suggesting that BM vessels express endothelial selectins constitutively and selectively. This interpretation is consistent with recent reports of E-selectin expression in noninflamed murine and human BM, detected by immunohistology or reverse-transcriptase PCR of noninflamed endothelial cells (8, 14), and with in vitro studies that have shown E-selectin–mediated rolling of human HPCs on cultured BM endothelial cells (8).

FDCP-mix Cells Interact with BM Microvessels in Mice Deficient in P/E-selectin. Although P- and E-selectin inhibition significantly reduced FDCP-mix cell rolling, the mAbs did not block interactions by >68%, even given in combination. To test whether rolling could occur in the complete absence of selectins, we used P/E-selectin doubly-deficient mice (14). Rolling of FDCP-mix cells in BM venules and sinusoids of these animals was lower than in wild-type littermates, consistent with a role for endothelial selectins in stem cell homing to BM. However, a significant fraction of cells continued to roll, and this interaction was not affected by inhibition of L-selectin (Fig. 2 *D*). Thus, additional selectin-independent adhesion mechanism(s) that are sufficient to support tethering and rolling of circulating HPCs in BM microvessels must exist.

Constitutively Expressed VCAM-1 Mediates Selectin-independent Rolling of FDCP-mix and M1 Progenitors in BM Microvessels. We hypothesized that VCAM-1 could be responsible for selectin-independent rolling. In vitro experiments have shown that VCAM-1 interaction with α4 integrins mediates lymphocyte tethering and rolling (31–33). Furthermore, immunohistochemical studies on sections of murine and human BM have shown that VCAM-1 is constitutively expressed in BM microvessels (7, 8). To determine whether VCAM-1 is present in murine skull caps, we injected fluoresceinated anti–VCAM-1 mAb (MK 2.7, F/P ratio 2.85) into mice. Within 10 min after injection, antibody accumulation was detectable at the luminal surface of BM venules and sinusoids (Fig. 3 *A*). In contrast, mAb binding was undetectable in most BV and in subdermal venules of the animals' ears, and BM vessels did not bind a mAb to the mucosal addressin MAdCAM-1 (MECA-367, F/P ratio 6.94; data not shown).

To test whether VCAM-1 and α4 integrins mediate FDCP-mix cell rolling, we used mAbs against these molecules. Both antibodies decreased rolling fractions in wild-type animals by 35–50% (Fig. 3 *B*), whereas rolling was inhibited by ~75% in P/E-selectin-deficient mice (Fig. 3 *C*), indicating that α4/VCAM-1 alone can initiate and sustain cell–cell interactions in BM venules and sinusoids. Both mAbs inhibited rolling equally, suggesting that other α4 ligands did not participate. Most of the rare cells that interacted with P/E-selectin-deficient BM vessels after inhibition of VCAM-1 rolled only briefly and typically detached within seconds, indicating that α4/VCAM-1 is the major selectin-independent rolling pathway.

Although α4-mediated rolling on purified, immobilized VCAM-1 or on transfectants is well documented (31–33), several in vitro studies of monocyte and T cell adhesion to endothelial monolayers were unable to demonstrate involvement of this pathway in rolling (33, 34). In these experiments, monocytes and T cells engaged with VCAM-1 only during firm adhesion and transendothelial migration. On the other hand, intravital microscopy studies of eosinophil and lymphocyte adhesion to inflamed mesenteric or cremaster muscle venules suggest that α4 integrins can support rolling in those tissues in synergy with, but not independent of, selectins (35–37). This variability in α4/VCAM-1–dependent adhesion could be due to several factors. First, the mode of VCAM-1 expression may vary. This may involve VCAM-1 surface density, ultrastructural presentation, host cell–specific posttranslational modification(s), or a combination of these factors. Although fluorescent signals from BM microvessels were partially absorbed by overlying tissues, and the skull itself emitted significant background fluorescence, labeled VCAM-1 mAb was readily visualized in BM microvessels, suggesting that VCAM-1 expression was high. Second, the differences may reflect variable levels of α4 affinity and/or avidity that may be host cell–dependent (38). However, rolling on VCAM-1 was not unique for FDCP-mix cells since rolling of the myeloid progenitor line M1 (16) was also blocked by anti-α4.

Endothelial Selectins and VCAM-1 Mediate Rolling of FL HPC in BM Microvessels. The fact that fluorescent VCAM-1 mAb was readily visualized in BM microvessels, even under conditions that are likely to render our method of detection relatively insensitive, suggests that VCAM-1 is ex-

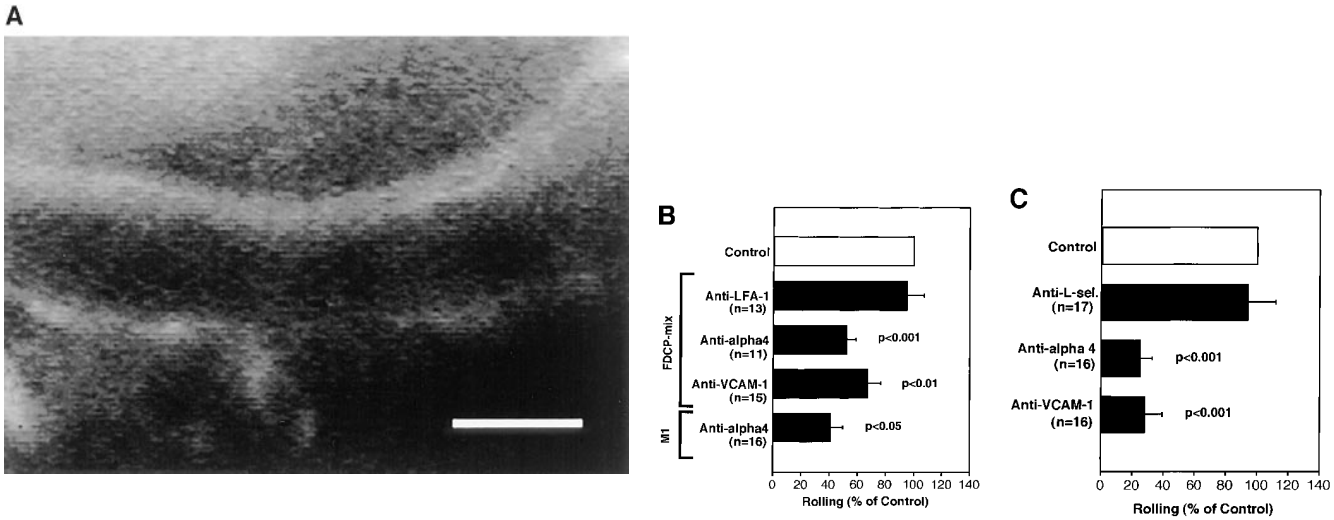

Figure 3. The α4/VCAM-1 pathway mediates selectin-independent rolling of progenitor cells in BM microvessels. (*A*) CFSE-labeled anti–VCAM-1 accumulation in a typical BM venule. 50 μg of fluorescently labeled mAb MK 2.7 was injected intravenously. 15 min later, the animal was anesthetized, the vena cava was cut, and the mouse was perfused through a catheter in the right common carotid artery with heparinized ice-cold saline to remove intravascular blood and unbound mAb. The optical plane was focused on the centerline of the venule revealing fluorescent mAb at the luminal surface of opposing vessel walls (*upward curved horizontal lines*). Scale bar depicts 50 μm. (*B* and *C*) Effect of mAbs against integrins and VCAM-1 in (*B*) wild-type mice and (*C*) P/E-selectin double knockout mice. Rolling fractions after mAb treatment were normalized to rolling fractions determined in the same vessel before mAb application (*control*). Only FDCP-mix cells were tested in P/E-selectin knockout animals. Groups were compared with control using the Kruskal-Wallis test with Bonferoni correction of *P* (for FDCP-mix cells) or the Student's two-tailed *t* test for paired data (for M1 cells). All data are shown as mean ± SEM of three independent experiments. *n*, number of venules per group.

pressed at considerable levels on the luminal surface of BM venules and sinusoids. Moreover, our studies with neutralizing mAbs clearly demonstrate that VCAM-1 mediates rolling of progenitor cell lines, presumably via interactions with $\alpha4\beta1$ (VLA-4). However, FDCP-mix and M1 cells express also $\alpha4\beta7$, which could have interacted weakly with VCAM-1. This integrin is absent on human (9) and murine (Mazo, I.B., and U.H. von Andrian, unpublished data) HPCs. Thus, although our studies with FDCP-mix cells demonstrate that $\alpha4$/VCAM-1 can mediate selectin-independent rolling in vivo, it could be argued that native HPCs may not be able to use this pathway because their $\alpha4$ integrins may have a different composition or functional activity.

Because it was not possible to isolate HPCs from adult mice at sufficient quantity and purity for in vivo experiments, we harvested FL cells from murine embryos at day 11 of gestation. HPCs from FLs were shown to home to the BM similarly to HPCs from adult BM (39). At day 11, murine FLs contain ~50% erythroid cells (Ter-119$^+$) and ~50% MNCs (Ter-119$^-$, c-kit$^+$) (40). Approximately half of the latter are uncommitted HPCs. The rest are bipotent progenitors of B cell/macrophage lineage (41). Flow cytometric analysis of FL cells confirmed these observations and revealed that Ter-119$^-$ c-kit$^+$ cells (HPCs) stained brightly with the fluorophore BCECF, whereas the fluorescence intensity of BCECF-labeled Ter-119$^+$ cells was 10–100-fold lower (data not shown). Control experiments revealed that most erythroid cells were thus below the detection threshold of our video camera. Therefore, we did not separate erythroid cells from HPCs because the latter constituted the vast majority (~90%) of detectable FL cells in BM vessels.

Rolling of FL HPCs in BM venules and sinusoids of wild-type mice was comparable to that of FDCP-mix cells (mean ± SEM of rolling fractions: 21.9 ± 4.9% for FL HPC vs. 19.9 ± 1.5% for FDCP-mix). Rolling was also markedly inhibited by anti–VCAM-1 (Fig. 4). Likewise, FL HPC rolling in P/E-selectin knockout mice was lower than in wild-type BM, and was nearly abolished after additional inhibition of VCAM-1. We conclude that FL HPC and likely other HPC populations behave equivalently to progenitor cell lines in that they are able to use either vascular selectins or the $\alpha4\beta1$/VCAM-1 pathway to initiate rolling. However, it should be noted that FL HPC, unlike progenitor cell lines, could be composed of different subpopulations whose rolling may be preferentially supported by one or the other mechanism.

Endothelial Specialization in BM Microvessels: Implications for HPC Homing. The parallel contribution by distinct constitutive rolling pathways in adult BM microvessels may function as a safeguard to provide access for circulating HPCs to areas where resident HPCs have been lost. It may similarly ensure sufficient seeding of the BM during fetal development. This could explain why a deficiency in P- and/or E-selectin or their fucosylated ligands does not abolish hematopoiesis in gene-targeted mice (14, 42). Similarly, a defect in fucose metabolism in humans with leukocyte adhesion deficiency syndrome type 2 causes a complete absence of selectin ligands resulting in increased susceptibility to infections (43). However, hematopoiesis in these patients is intact, presumably because HPCs can still use $\alpha4$/VCAM-1 to reach the BM.

A similar evaluation of $\alpha4$ or VCAM-1 in gene-targeted mice is more complex because either null mutation is embryonic lethal before the BM is formed (44). However, hematopoiesis has been examined in animals that express a hypomorphic VCAM-1 mutant (1), and in chimeric mice that lack $\alpha4$ integrins on hematopoietic cell subsets (45). Together, these studies indicate that defects in endothelial selectins or in $\alpha4$/VCAM-1 can lead to abnormalities in blood cell production or differentiation, but neither of these pathways alone is essential for HPC homing to the BM. Our findings are consistent with this interpretation; endothelial selectins and VCAM-1 could independently initiate and sustain HPC adhesion in BM venules and sinusoids.

HPC migration from FL to BM during fetal development occurs in a sterile uterine environment and involves a large number of HPCs that colonize the BM during ongoing extramedullary hematopoiesis (39). In contrast, patients undergoing BM ablation for HPC transplantation are not similarly well protected. Intravenously transplanted HPCs are likely to use the same adhesion pathways to reach hematopoietic compartments in the BM. Indeed, antibodies to VCAM-1 and/or $\alpha4$ were shown to reduce the number of homed HPCs in the BM of lethally irradiated mice by ~50% (5). The partial preservation of HPC homing in these experiments is consistent with a contribution by P- and E-selectin, but the role of endothelial selectins in hematopoietic recovery after HPC transplantation has not been examined so far. A clinical study has reported that the number of L-selectin^{hi} HPCs in BM grafts correlated with faster recovery of thrombopoiesis (10), but it is unclear whether this is an effect of differential HPC migration. Our observations suggest that L-selectin does not contribute to HPC homing, at least in unchallenged BM. It is possible that conditioning with chemotherapy or irradiation before transplantation may induce changes in BM endothelial cells (7). However, a recent report has shown that short-term homing of HPCs to irradiated BM is lower than to untreated BM (46). Thus, it is unclear whether irradiation promotes HPC seeding of the BM because of enhanced HPC recruitment from the blood or because of other effects such as an increased accessibility of extravascular sites that promote HPC survival and hematopoiesis.

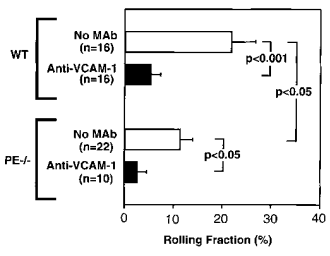

Figure 4. Fluorescently labeled HPC from day 11 FLs of C57/B6J embryos were analyzed in BM microvessels of wild-type and P/E-selectin–deficient mice before and after treatment with anti–VCAM-1 (100 μg/mouse). Data in wild-type mice are from three independent experiments. FL HPC rolling was determined in three P/E-selectin-deficient mice, and one of these animals was additionally treated with anti–VCAM-1. All bars depict mean ± SEM. *n*, number of venules. Groups were compared using Student's *t* test for paired or unpaired data where appropriate.

Nevertheless, it appears reasonable that the kinetics of hematopoietic recovery after HPC transplantation correlate with the efficacy of HPC homing to the BM, particularly when the number of HPCs is limited. Thus, a defect or reduced efficacy of selectin ligands or $\alpha 4\beta 1$ might reduce HPC homing and prolong the period during which patients are at risk of infection or bleeding. This could be particularly important for therapies using highly purified autologous HPCs or transfected HPCs as a treatment of cancer or genetic deficiencies. Methods of transfection and cultivation of HPCs have been reported (47, 48), but the effects of these manipulations on HPC expression of selectin ligands and $\alpha 4\beta 1$ have not been examined. Based on our findings, we speculate that culture conditions or other manipulations that preserve or enhance the ability of HPCs to interact with vascular selectins or VCAM-1 may have beneficial effects on the homing of transfused cells to a recipient's BM.

In conclusion, our experiments assign a pivotal function to P/E-selectin and VCAM-1 as endothelial determinants that initiate adhesion between BM endothelial cells and circulating HPCs. However, our findings do not exclude a role for chemoattractants or other adhesion molecules that may be critical for firm arrest of rolling cells or subsequent diapedesis. Indeed, unique combinations of rolling receptors, chemoattractants, and secondary adhesion molecules direct the specific migration of differentiated myeloid and lymphoid cells to other organs (3, 4, 49). While some molecules participate in many adhesion cascades, others function selectively in specialized vascular beds such as the high endothelial venules of peripheral lymph nodes and Peyer's patches (49). These so-called vascular addressins constitute a single molecular species or antigenic determinant and act as highly efficient rolling receptors. The adhesion-initiating vascular addressins of the BM differ from their counterparts in high endothelial venules inasmuch as they are not a single endothelial determinant but a unique combination of adhesion molecules that appear to make equivalent parallel contributions during HPC homing.

We thank Drs. E.C. Butcher and B. Wolitzky for providing antibodies; Dr. A. Peled for providing M1 cells; and B. Fors and G. Cheng for excellent technical assistance. We are grateful to Dr. C. Lloyd for her help in histology assay, and to M. Ryan for expert assistance in flow cytometry. Special thanks to Dr. E. Quackenbush for her advice in experiments with FL cells.

This work was supported by National Institutes of Health grants HL-54936 and HL-56949.

Address correspondence to Ulrich H. von Andrian, The Center for Blood Research, 200 Longwood Ave., Boston, MA 02115. Phone: 617-278-3130; Fax: 617-278-3190; E-mail: uva@cbr.med.harvard.edu

Received for publication 31 March 1998.

References

1. Friedrich, C., M.I. Cybulsky and J.C. Gutierrez-Ramos. 1996. Vascular cell adhesion molecule-1 expression by hematopoiesis-supporting stromal cells is not essential for lymphoid or myeloid differentiation in vivo or in vitro. *Eur. J. Immunol.* 26:2773–2780.
2. Papayannopoulou, T., and B. Nakamoto. 1993. Peripheralization of hemopoietic progenitors in primates treated with anti-VLA4 integrin. *Proc. Natl. Acad. Sci. USA.* 90:9374–9378.
3. Butcher, E.C. 1991. Leukocyte-endothelial cell recognition: three (or more) steps to specificity and diversity. *Cell.* 67: 1033–1036.
4. Springer, T.A. 1994. Traffic signals for lymphocyte recirculation and leukocyte emigration: the multi-step paradigm. *Cell.* 76:301–314.
5. Papayannopoulou, T., C. Craddock, B. Nakamoto, G.V. Priestley, and N.S. Wolf. 1995. The VLA4/VCAM-1 adhesion pathway defines contrasting mechanisms of lodgement of transplanted murine hemopoietic progenitors between bone marrow and spleen. *Proc. Natl. Acad. Sci. USA.* 92:9647–9651.
6. Tavassoli, M., and C.L. Hardy. 1990. Molecular basis of homing of intravenously transplanted stem cells to the marrow. *Blood.* 76:1059–1070.
7. Jacobsen, K., J. Kravitz, P.W. Kincade, and D.G. Osmond. 1996. Adhesion receptors on bone marrow stromal cells: in vivo expression of vascular cell adhesion molecule-1 by reticular cells and sinusoidal endothelium in normal and γ-irradiated mice. *Blood.* 87:73–82.
8. Schweitzer, K.M., A.M. Drager, P. van der Valk, S.F. Thijsen, A. Zevenbergen, A.P. Theijsmeijer, C.E. van der Schoot, and M.M. Langenhuijsen. 1996. Constitutive expression of E-selectin and vascular cell adhesion molecule-1 on endothelial cells of hematopoietic tissues. *Am. J. Pathol.* 148:165–175.
9. Friedrich, C., and J.C. Gutierrez-Ramos. 1995. Characterization of adhesion receptors expressed on cord blood $CD34^+$ cells. *In* Leukocyte Typing V. S.F. Schlossman, L. Boumsell, W. Gilks, J.M. Harlan, T. Kishimoto, C. Morimoto, J. Ritz, S. Shaw, R. Silverstein, T. Springer, T.F. Tedder, and R.F. Todd, editors. Oxford University Press, Oxford, UK. 1637–1639.
10. Dercksen, M.W., W.R. Gerritsen, S. Rodenhuis, M.K. Dirkson, I.C. Slaper-Cortenbach, W.P. Schaasberg, H.M. Pinedo, A.E. von dem Borne, and C.E. van der Schoot. 1995. Expression of adhesion molecules on $CD34^+$ cells: $CD34^+$ L-selectin$^+$ cells predict a rapid platelet recovery after peripheral blood stem cell transplantation. *Blood.* 85:3313–3319.
11. Griffin, J.D., O. Spertini, T.J. Ernst, M.P. Belvin, H.B. Levine, Y. Kanakura, and T.F. Tedder. 1990. GM-CSF and other cytokines regulate surface expression of the leukocyte adhesion molecule-1 (LAM-1) on human neutrophils, monocytes, and their precursors. *J. Immunol.* 145:576–584.
12. Arbonès, M.L., D.C. Ord, K. Ley, H. Ratech, C. Maynard-Curry, G. Otten, D.J. Capon, and T.F. Tedder. 1994. Lymphocyte homing and leukocyte rolling and migration are im-

paired in L-selectin–deficient mice. *Immunity*. 1:247–260.
13. Zannettino, A.C., M.C. Berndt, C. Butcher, E.C. Butcher, M.A. Vadas, and P.J. Simmons. 1995. Primitive human hematopoietic progenitors adhere to P-selectin (CD62P). *Blood*. 85:3466–3477.
14. Frenette, P.S., T.N. Mayadas, H. Rayburn, R.O. Hynes, and D.D. Wagner. 1996. Susceptibility to infection and altered hematopoiesis in mice deficient in both P- and E-selectins. *Cell*. 84:563–574.
15. Spooncer, E., C.M. Heyworth, A. Dunn, and T.M. Dexter. 1986. Self-renewal and differentiation of interleukin-3–dependent multipotent stem cells are modulated by stromal cells and serum factors. *Differentiation*. 31:111–118.
16. Benayahu, D., A. Peled, and D. Zipori. 1994. Myeloblastic cell line expresses osteoclastic properties following coculture with marrow stromal adipocytes. *J. Cell. Biochem*. 56:374–384.
17. von Andrian, U.H. 1996. Intravital microscopy of the peripheral lymph node microcirculation in mice. *Microcirculation*. 3:287–300.
18. Pries, A.R. 1988. A versatile video image analysis system for microcirculatory research. *Int. J. Microcirc. Clin. Exp*. 7:327–345.
19. Ley, K., and P. Gaehtgens. 1991. Endothelial, not hemodynamic, differences are responsible for preferential leukocyte rolling in rat mesenteric venules. *Circ. Res*. 69:1034–1041.
20. Branemark, P.I. 1959. Vital microscopy of bone marrow in rabbit. Ph. D. thesis. Berlingska Boktryckeriet, Lund. 82 pp.
21. De Bruyn, P.P.H., S. Michelson, and T.B. Thomas. 1971. The migration of blood cells of the bone marrow through the sinusoidal wall. *J. Morphol*. 133:417–438.
22. Johnson, L.V., M.L. Walsh, B.J. Bockus, and L.B. Chen. 1981. Monitoring of relative mitochondrial membrane potential in living cells by fluorescence microscopy. *J. Cell Biol*. 88:526–535.
23. Bertoncello, I., G.S. Hodgson, T.R. Bradley, S.D. Hunter, and L. Barber. 1985. Multiparameter analysis of transplantable hemopoietic stem cells: I. The separation and enrichment of stem cells homing to marrow and spleen on the basis of rhodamine-123 fluorescence. *Exp. Hematol*. 13:999–1006.
24. Kansas, G.S. 1996. Selectins and their ligands: current concepts and controversies. *Blood*. 88:3259–3287.
25. Sako, D., X.-J. Chang, K.M. Barone, G. Vachino, H.M. White, G. Shaw, G.M. Veldman, K.M. Bean, T.J. Ahern, B. Furie, et al. 1993. Expression cloning of a functional glycoprotein ligand for P-selectin. *Cell*. 75:1179–1186.
26. Berg, E.L., M.K. Robinson, O. Mansson, E.C. Butcher, and J.L. Magnani. 1991. A carbohydrate domain common to both sialyl Le^a and sialyl Le^x is recognized by the endothelial cell leukocyte adhesion molecule ELAM-1. *J. Biol. Chem*. 266:14869–14872.
27. Ley, K., D.C. Bullard, M.L. Arbonés, R. Bosse, D. Vestweber, T.F. Tedder, and A.L. Beaudet. 1995. Sequential contribution of L- and P-selectin to leukocyte rolling in vivo. *J. Exp. Med*. 181:669–675.
28. Fiebig, E., K. Ley, and K.E. Arfors. 1991. Rapid leukocyte accumulation by "spontaneous" rolling and adhesion in the exteriorized rabbit mesentery. *Int. J. Microcirc. Clin. Exp*. 10:127–144.
29. Kubes, P., and D.N. Granger. 1996. Leukocyte-endothelial cell interactions evoked by mast cells. *Cardiovasc. Res*. 32:699–708.
30. Bevilacqua, M.P., S. Stengelin, M.A. Gimbrone, Jr., and B. Seed. 1989. Endothelial leukocyte adhesion molecule 1: an inducible receptor for neutrophils related to complement regulatory proteins and lectins. *Science*. 243:1160–1165.
31. Berlin, C., R.F. Bargatze, U.H. von Andrian, M.C. Szabo, S.R. Hasslen, R.D. Nelson, E.L. Berg, S.L. Erlandsen, and E.C. Butcher. 1995. α4 integrins mediate lymphocyte attachment and rolling under physiologic flow. *Cell*. 80:413–422.
32. Alon, R., P.D. Kassner, M.W. Carr, E.B. Finger, M.E. Hemler, and T.A. Springer. 1995. The integrin VLA-4 supports tethering and rolling in flow on VCAM-1. *J. Cell Biol*. 128:1243–1253.
33. Jones, D.A., L.V. McIntire, C.W. Smith, and L.J. Picker. 1994. A two-step adhesion cascade for T cell/endothelial cell interactions under flow conditions. *J. Clin. Invest*. 94:2443–2450.
34. Luscinskas, F.W., G.S. Kansas, H. Ding, P. Pizcueta, B.E. Schleiffenbaum, T.F. Tedder, and M.A. Gimbrone, Jr. 1994. Monocyte rolling, arrest and spreading on IL-4–activated vascular endothelium under flow is mediated via sequential action of L-selectin, β_1-integrins, and β_2-integrins. *J. Cell Biol*. 125:1417–1427.
35. Sriramarao, P., U.H. von Andrian, E.C. Butcher, M.A. Bourdon, and D.H. Broide. 1994. L-selectin and very late antigen-4 integrin promote eosinophil rolling at physiological shear rates in vivo. *J. Immunol*. 153:4238–4246.
36. Kanwar, S., D.C. Bullard, M.J. Hickey, C. Wayne Smith, A.L. Beaudet, B.A. Wolitzky, and P. Kubes. 1997. The association between α_4-integrin, P-selectin, and E-selectin in an allergic model of inflammation. *J. Exp. Med*. 185:1077–1087.
37. Johnston, B., T.B. Issekutz, and P. Kubes. 1996. The α_4-integrin supports leukocyte rolling and adhesion in chronically inflamed postcapillary venules in vivo. *J. Exp. Med*. 183: 1995–2006.
38. Lévesque, J.-P., D.I. Leavesley, S. Niutta, M. Vadas, and P.J. Simmons. 1995. Cytokines increase human hemopoietic cell adhesiveness by activation of very late antigen (VLA)-4 and VLA-5 integrins. *J. Exp. Med*. 181:1805–1815.
39. Zanjani, E.D., J.L. Ascensao, and M. Tavassoli. 1993. Liver-derived fetal hematopoietic stem cells selectively and preferentially home to the fetal bone marrow. *Blood*. 81:399–404.
40. Sanchez, M.-J., A. Holmes, C. Miles, and E. Dzierzak. 1996. Characterization of the first definitive hematopoietic stem cells in the AGM and liver of the mouse embryo. *Immunity*. 5:513–525.
41. Delassus, S., and A. Cumano. 1996. Circulation of hematopoietic progenitors in the mouse embryo. *Immunity*. 4:97–106.
42. Maly, P., A.D. Thall, B. Petryniak, C.E. Rogers, P.L. Smith, R.M. Marks, R.J. Kelly, K.M. Gersten, G. Cheng, T.L. Saunders, et al. 1996. The α(1,3) fucosyltransferase Fuc-TVII controls leukocyte trafficking through an essential role in L-, E-, and P-selectin ligand biosynthesis. *Cell*. 86:643–653.
43. Etzioni, A., M. Frydman, S. Pollack, I. Avidor, M.L. Phillips, J.C. Paulson, and R. Gershoni-Baruch. 1992. Recurrent severe infections caused by a novel leukocyte adhesion deficiency. *N. Engl. J. Med*. 327:1789–1793.
44. Hynes, R.O. 1996. Targeted mutations in cell adhesion genes: what have we learned from them? *Dev. Biol*. 180: 402–412.
45. Arroyo, A.G., J.T. Yang, H. Rayburn, and R.O. Hynes. 1996. Differential requirements for α4 integrins during fetal and adult hematopoiesis. *Cell*. 85:997–1008.
46. Hendrikx, P.J., C.M. Martens, A. Hagenbeek, J.F. Keij, and J.W. Visser. 1996. Homing of fluorescently labeled murine hematopoietic stem cells. *Exp. Hematol*. 24:129–140.
47. Berardi, A.C., A. Wang, J.D. Levine, P. Lopez, and D.T. Scadden. 1995. Functional isolation and characterization of human hematopoietic stem cells. *Science*. 267:104–108.
48. Mulligan, R.C. 1993. The basic science of gene therapy. *Science*. 260:926–932.
49. Butcher, E.C., and L.J. Picker. 1996. Lymphocyte homing and homeostasis. *Science*. 272:60–66.